

Climbing Cam Analysis

ME 478
Fall 2007

Justin Reina
Matt Kim

Introduction

Finite element analysis, or FEA, is used to find the forces throughout a structure given external forces and constraints. By finding the forces in a structure, an engineer can optimize a design prior to beginning its fabrication. The design can be tested and analyzed numerically. Maximum stresses are found and material is added and removed appropriately to improve the design. Deformed shape is found and used to determine whether or not a design is acceptable.

In the climbing industry there are two principal concerns: safety and weight. Equipment needs to be light so it does not weigh climbers down. While weight is an important factor in climbing gear, the most important is strength. If a climbing gear fails during use, it can have deadly consequences. Clearly this is an area where FEA can and should be used as part of the design process.

A climbing cam, more specifically a #5 Black Diamond Camalot, was modeled and an FEA solution was found for a typical loading situation. Stress concentrations could clearly be seen along with areas that contained more material than necessary. To simplify analysis, a single lobe of the cam was analyzed.

FEA solution is not exact and a number of factors, including element type, mesh density, and the correct computer model, can influence the final solution. Thus, the final FEA solution must be verified. For this report, the FEA solution was verified with two different methods. Experimental strain data was collected for a numerical comparison of stress values at a single point. Additionally, a photo elastic test was conducted for a qualitative confirmation of the FEA solution for the entire cam model.

Specimen Description



Figure 1: Photograph of #5 Black Diamond Camelot. Courtesy of Black Diamond Ltd.

Climbing cams are used to protect climbers from gravity and death. They are inserted into cracks and can support the immense loads caused by falling and hauling gear. By deflecting and amplifying loads outwards, cams generate friction between their lobes and the sides of the crack they are placed in. The outward force the cam creates is generated by the angle between the axle of the cam and the point on the surface of the lobe that contacts the crack. This angle, called the camming angle, is forced to be constant throughout the cams range by carefully designing the shape of the cam. This shape takes the form of a logarithmic spiral shown in Eq. 1.

$$R = R_0 e^{\theta \tan \beta} \quad (1)$$

Where R is the radius, θ is the angle of rotation of the cam, R_0 is the radius for an angle of zero, and β is the camming angle. The camming angle was measured at 13 degrees. A plot of radius and cam angle can be seen in Fig. 2

A logarithmic spiral ensures a constant cam angle throughout the cams operating range. With the cam angle determined, simple calculations were used to determine the reaction forces. The cam cannot resist moments, thus the forces act along the line between the contact point and the cam axle as shown in Fig 3.

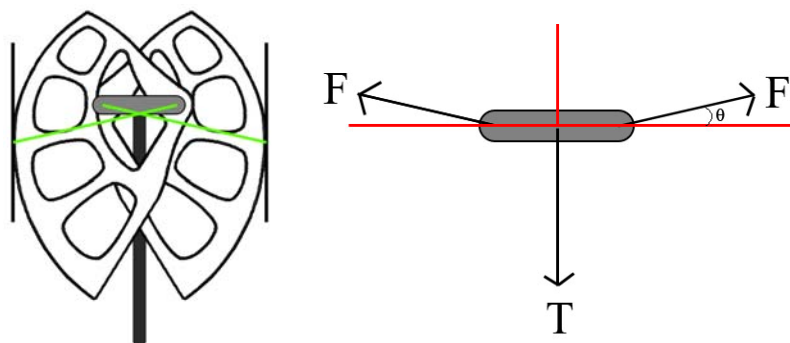


Figure 2: Climbing cam geometry. Left: green line shows the axis that the force vector must be on. Right: Free Body Diagram of the center linkage. T is the downward force on the cam.

Using the FBD in Fig. 3, the relation for the components of force acting on the cam is shown in Eq. 1-4. Since there are four cam lobes on a climbing cam, the loads are distributed.

$$\Sigma F_y = 4F_y - T = 0 \quad (1)$$

$$F_y = \frac{1}{4}T \quad (2)$$

$$F_x = \frac{\frac{1}{4}T}{\tan \theta} \quad (3)$$

$$F_{1x} = 1.083T \quad (4)$$

Experimental Results

A physical test of the climbing cam was conducted to validate the FEA solution. This test was focused on obtaining numerical values that can be used to validate the ANSYS model. Strains were measured at a point as the load on the cam was increased. This provided numerical values for strain that could be compared to the numerical values obtained through ANSYS.

The cam was tested on an Instron 5585H Load Frame as shown in Fig. 4. The Instron Load Frame specifications are shown in Table 1.

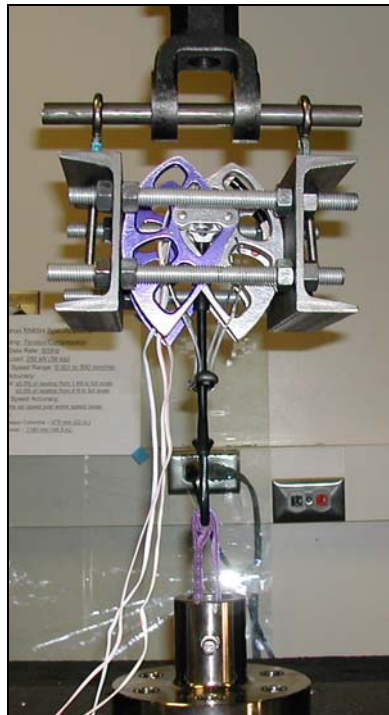


Figure 3: Photograph of test setup. The climbing cam is positioned in between the Instron test jig.

Table 1: Instron 5585H Load Frame Specifications

Static Loading	Tension/Compression
Max Data Rate (Hz)	500
Max Load (kN)	250
Crosshead Speed (mm/min)	0.001 - 500
Load Cell Accuracy - 250 kN	±0.5%
Load Cell Accuracy - 1 kN	±0.5%
Width between column (mm)	575
Vertical Travel (mm)	1180

A pair of parallel surfaces was needed to simulate a rock crevice for the test. An Instron jig was created with two C channels plates and four all thread rods. Four all thread rods were bolted into holes drilled into the C channel. Two eye bolts were bolted to the top of the C channel. The test

jig was attached to the Instron machine through a solid bar running across the eye bolts. The test jig is shown in Fig. 4. For the test, the C channels were set 4.7 inches apart, which is near the middle of the cam's range.

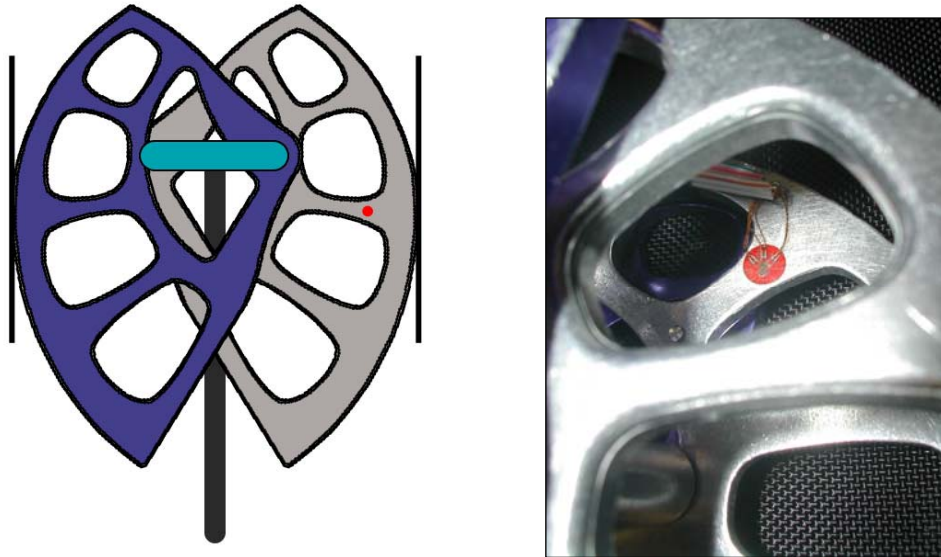


Figure 4: Location of the strain gage. Left: 2D representation of test setup. The vertical lines on the side represent the rigid test plate surface. The red dot indicated the location of the strain gage. There is a downward force exerted in the center. Right: Photograph of strain gage location.

A rectangular strain rosette was used to measure the strain in the cam. It was attached to the flat inner surface of the silver cam lobe along the middle web located across from the contact point. The location of the strain gage is marked with a red dot in Fig. 5. The strain gage was manufactured by Tokyo Sokki Kenkyujo Co. Ltd. The strain gage properties are shown in Table 2.

Table 2: Strain gage specification. Courtesy of Tokyo Sokki Kenkyujo Co., Ltd.

Gage Type	FRA-6-23
Gage Length (mm)	6
Gage Width (mm)	2.4
Backing Diameter (mm)	14
Resistance (Ω)	120
Adhesive	P-2
Gage Factor	$2.14 \pm 1\%$
Coefficient of Thermal Expansion ($1/^\circ\text{C}$)	$2.30\text{E-}05$
Temperature Coefficient of GF ($\%/10^\circ\text{C}$)	0.1 ± 0.05

The cam was set between the plates. It was then given a quick jerk to allow the cams to wedge into the test plates. The cam was anchored to the base of the Instron. The Instron software was used to measure the force while a separate computer was used to collect the strain data.

The test jig was raised up as the tensile force was increased in 100 N increments. Ten strain measurements were collected over two seconds at each load step. The strain measurements were then averaged for the analysis. The average strain data is listed in Appendix B.

The strain measurements were transformed into strains in the global coordinate system using Eqs. 5-8.

$$\varepsilon_x = 2\left(\varepsilon_1 + \frac{\varepsilon_3 - \varepsilon_1}{2}\right) - \varepsilon_2 \quad (5)$$

$$\varepsilon_y = \varepsilon_2 \quad (6)$$

$$\varepsilon_{xy} = \varepsilon_1 - \varepsilon_2 + \varepsilon_3 \quad (7)$$

$$\gamma_{xy} = 2\varepsilon_{xy} \quad (8)$$

Plane stress assumption was used to solve for the stresses. The matrix equation for plane stress is shown in Eq. 9. Plane stress assumption is appropriate since the out of plane stress at the location of the strain gage is zero. The applied force occurs only in the plane of the cam.

$$\begin{bmatrix} \sigma_x \\ \sigma_y \\ \tau_{xy} \end{bmatrix} = \frac{E}{1-\nu^2} \begin{bmatrix} 1 & \nu & 0 \\ \nu & 1 & 0 \\ 0 & 1/2 & -\nu \end{bmatrix} \begin{bmatrix} \varepsilon_x \\ \varepsilon_y \\ \gamma_{xy} \end{bmatrix} \quad (9)$$

According to Black Diamond's website, the cams are made from 7075 aluminum. The material properties, shown in Table 3, were used to solve for the stress.

Table 3: Material Properties for 7075 Al. (Courtesy of Matweb.com).

E (GPa)	72
ν	0.33

The stresses were converted into von Mises effective stress using Eq. 10.

$$\sigma_e = \frac{1}{\sqrt{2}} \sqrt{(\sigma_x - \sigma_y)^2 + (\sigma_x)^2 + (\sigma_y)^2 + 6(\tau_{xy})^2} \quad (10)$$

The effective stress from the strain gage data is plotted in Fig. 6.

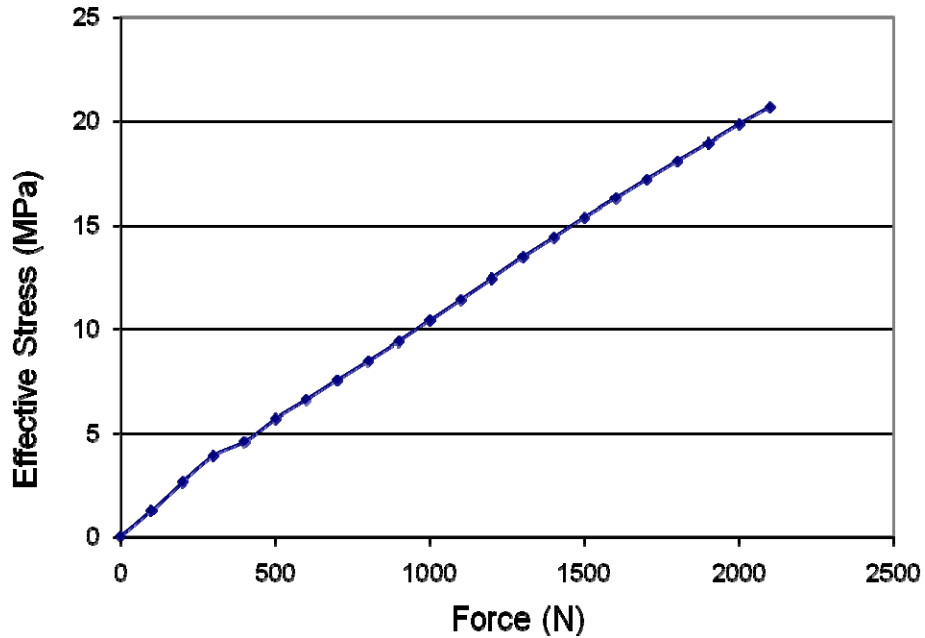


Figure 5: *Experimental effective stress at the strain gage location.*

The graph shows a linear relation between the force and the stress. This is expected since the cam was loaded within its elastic region. There is a small slope change between 300 N and 400 N of force. This may indicate that the climbing cam resettled to a new equilibrium angle during the test. The slope of the stress is relatively constant after 500 N.

Photoelastic Results

Photoelastic testing was used to provide qualitative validation of the FEA solution. Using a plastic model of the climbing cam with the same geometry is appropriate for qualitative analysis. Both materials are used within the elastic region and thus, the stress fields are only dependent on the geometry and loading condition.

The photoelastic model was created from Homalite H-911 CR-39® plastic sheet. It was cut with a waterjet using the same CAD file that was used for the ANSYS analysis. The waterjet process created smooth edges and left very little residual stress on the model. A small crack was created on the edge of the center cutout during cutting. The presence of this crack created additional stress fields during the photoelastic test. A picture of the photoelastic model is shown in Fig. 7.



Figure 6: Image of Photoelastic model. Made from Homalite H-911 CR-39® plastic sheet.

The photoelastic model was placed in between the Instron jig that was used for the experimental test. The cam was pinned at the bottom with an L shaped bar. The load on the cam was exerted by lowering the test jig plate down slowly on the top of the cam. A diagram of the photoelastic test setup is shown in Fig. 8.

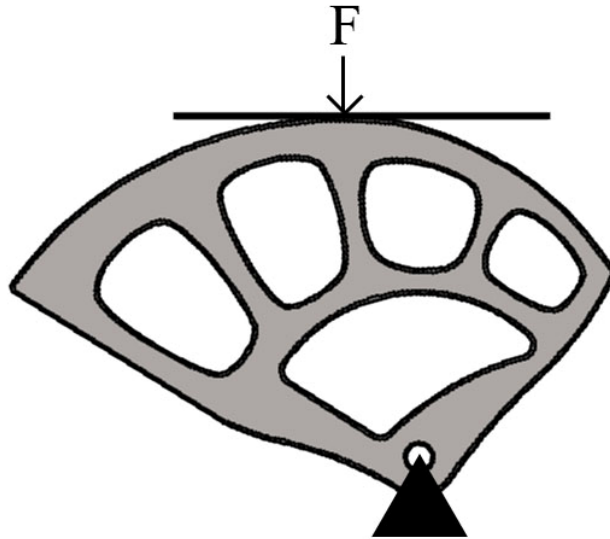


Figure 7: Photoelastic test setup. The cam is pinned at the bottom and a downward force is exerted by a plate on top of the cam.

The photoelastic images were captured as the downward force on the cam was increased. The images from the photoelastic test are shown in Fig. 9.

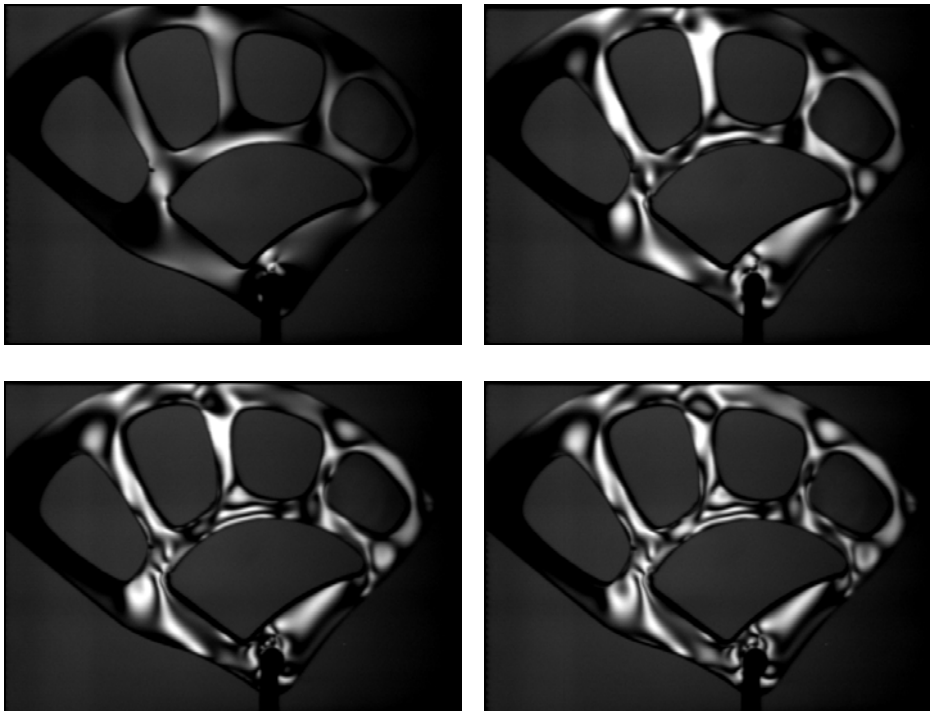


Figure 8: Progression of forces as photoelastic cam is compressed. Progression from top left to bottom right.

Many fringes lines, lines between dark and light areas, can be seen in Fig. 9. The fringe lines in the model are chaotic and difficult to count with great accuracy. These fringes are directly correlated to the difference between the first and second principal stresses as shown in Eq. 11.

$$\sigma_1 - \sigma_2 = \frac{f}{t} \bar{N} \quad (11)$$

Where, \bar{N} is the *isochromatic fringe order*, f is the stress-optical coefficient, t is the model thickness, and σ_1 and σ_2 are the first and second principal stresses. Since f and t are constants, the difference between the first and second principal stresses is indicated by the number of fringes that can be seen.

The stress-optical coefficient was not obtained for this report because obtaining numerical values of stress through the photoelastic test was outside the scope of this report. Knowing that the number of lines is directly correlated the maximum shear stress was enough to validate the ANSYS solution. Regions of high strain will have numerous fringes while regions of low strain will have a smaller number of broader lines.

In the final exposure, shown in Fig 10, the fringes are concentrated along the three center cam webs and the middle arc. Also, regions of high fringes can be seen around the axle and at the area of loading. Regions of low stress can be seen in the left and right ends of the cam. Compared with other webs, the left most one that attaches to the axle appears to be a region of low stress.

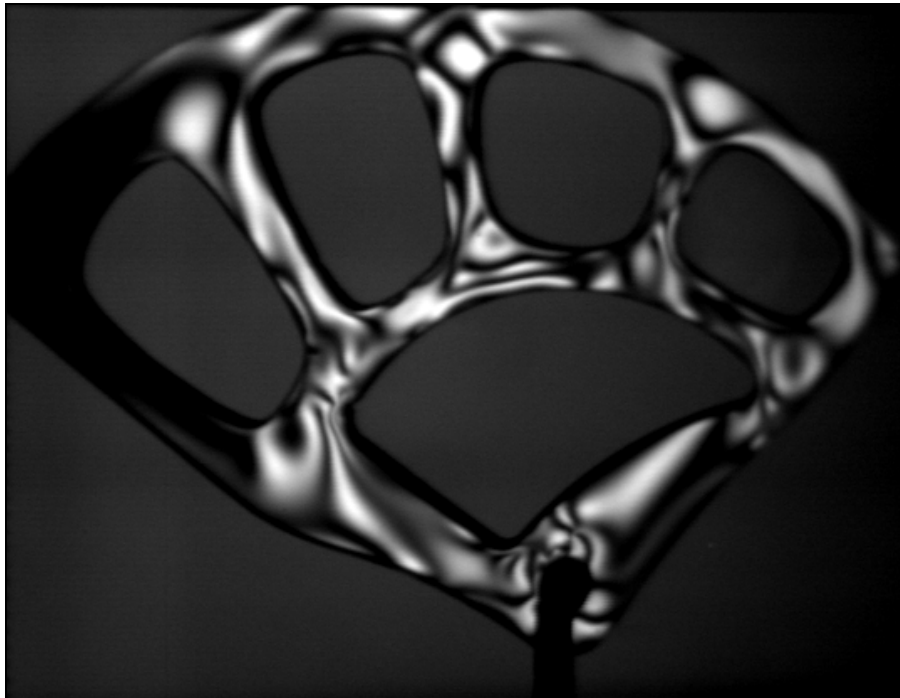


Figure 9: Photoelastic cam at maximum loading. Higher loading was not used for fear of destroying the model, which may be used in future classes.

The photoelastic results will be compared to the stress fields generated by ANSYS later in this report.

Analytical Methodology

To develop a better understanding of the FE solution process, several different modeling options were explored. As novice users, the first derived model would be the simplest, a planar representation of the cam lobe. This model is valid as it has a uniform thickness and all loads are presented in-plane with the two-dimensional model. The model is shown in Fig. 11.

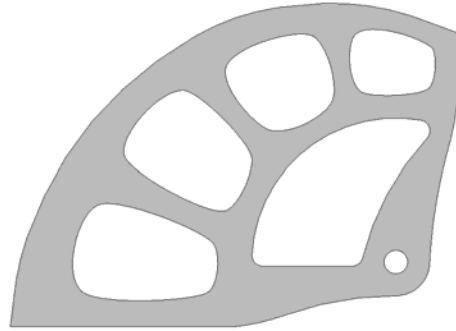


Figure 10: *Planar Cam Lobe Model.*

The chosen element for this model was the eight-noded quadrilateral element with thickness, due to its ability to represent curved boundaries with higher precision than four-noded quadrilaterals.

This model would first be explored for convergence, by examining the effective stresses at a point for several mesh sizes. The ‘Mesh Tool’ would be utilized in this analysis as its method of refinement will result in a lower error mesh than establishing a constant element edge length parameter. Meshes were performed until satisfactory results were achieved to establish convergence.

The two-dimensional model would then be explored for accuracy with respect to experimental results. This would first involve comparing the strain at a point. Next, a more general comparison of stress fields would be examined for the planar model.

A three-dimensional model of the cam lobe would next be explored. This model in theory is equivalent to a planar model with thickness, and the hypothesis of equivalency would next be tested. The element of choice for the three-dimensional model was the ten-noded tetrahedral element. The three-dimensional model is as follows:

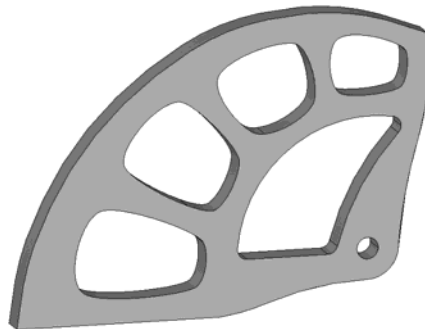


Figure 11: *Three Dimensional Cam Model.*

Analytical Procedure

Planar Model Loading

Loading of the planar modeling was first achieved by identifying the force acting on the cam lobe. This was calculated from Eq. 2 and Eq. 4. These values, F_x and F_y , were then applied as point loads on the pin hole. Only nodes located on the half of the hole facing the contact location were selected to simulate true contact force. The following is an illustration of the process:

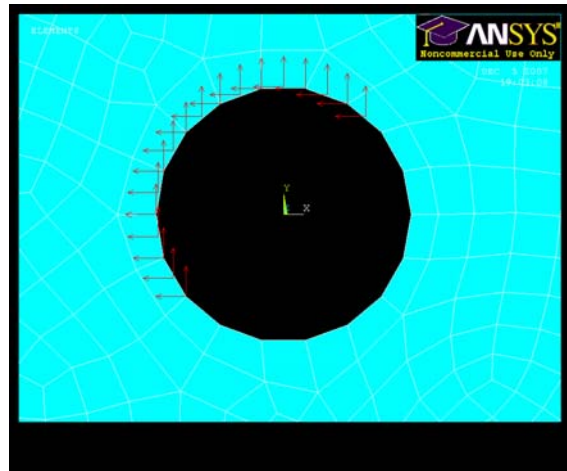


Figure 12: Applied Load as Vector Components to the Cam Pin Location.

Point loads were also equally weighted to simulate the actual load. To model the wall contact, displacement constraints were imposed on the region of cam contact with the wall. This worked well for simulating reactions away from the wall, however it was noted that this created false stress concentrations near this displacement constraint.

Solid Model Loading

Solid model loading was accomplished in the same manner as the planar model, although it provided a significantly higher degree of difficulty within the ANSYS interface.

FE analysis was conducted on two and three-dimensional models. Analysis was first performed on the two-dimensional models.

Planar Model Generation

The planar model was first imported into the ANSYS interface. Eight-noded quadrilateral elements were used for the lobe and the Mesh Tool was utilized to generate a minimal error mesh. This was the general procedure for planar meshes.

Convergence Testing

Convergence of the FE results was tested by examining the effective stress at a point in the cam lobe. This point was as follows:

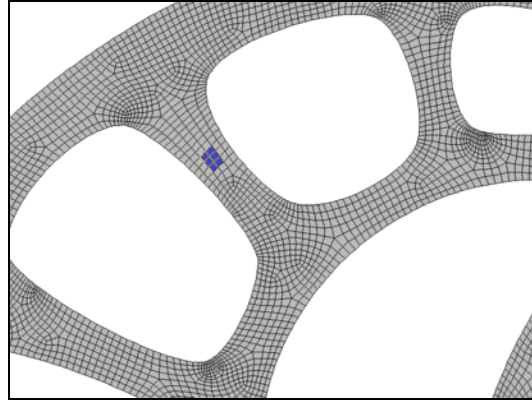


Figure 13: Location for Convergence on Planar Model.
Element Mesh shown is highest tested mesh (5747 elements).

This location was chosen due to its predicted approximate uniaxial state of stress. Thus lower element meshes in this area should in theory result in minimal error in comparison to higher complexity regions of stress.

The element numbers in Fig. 14 were recorded and tests were performed for meshes ranging from 9 to 1 using the ‘*Smart Mesh*’ feature of the ‘*Mesh Tool*’. An additional test was performed using the ‘*Refine At*’ feature on the ‘*Smart Mesh*’ value of 1.

For each mesh, the load was applied and displacement constraints fixed.

The effective stresses for each mesh were then outputted in an element table, and the specific convergence location elements were recorded.

Graphical results were also obtained by first examining the highest density mesh. An element plot was displayed of the effective stress and the scale used for the stress scale used for this model recorded, to be used for all subsequent meshes.

Graphical and numerical results were then taken for *Smart Mesh* values of 9, 7, 6, 5, 4, 3, 2, 1, and also of a refined mesh of *Smart Mesh* 1.

Strain Gauge Verification – Planar Model

To obtain strain gauge results from the planar model, the location of the strain gauge was first determined. This was accomplished by inserting a reference circle designating the location of the gauge into the meshed planar model, as follows:



Figure 14: Location of experimental gauge location

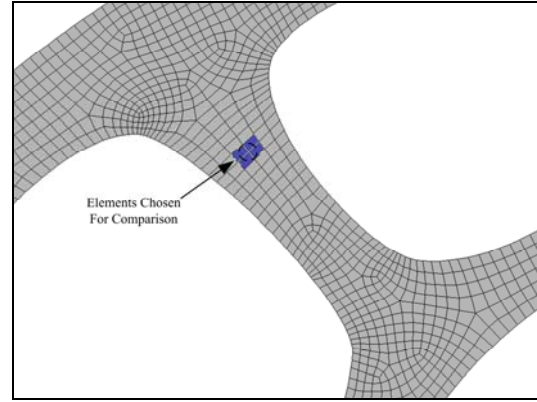


Figure 15: ANSYS approximation of gauge location.

The planar model was then loaded to the equivalent maximum experimental load and properly constrained. Numerical results for the effective stresses were obtained for elements found in Fig. 16. Results were averaged, and statistics recorded. This value was then extrapolated as the effective stress for the strain gauge as a function of cam handle loading.

Photoelastic Verification

To verify the Photoelastic experimental results in absence of material specifications and loading data, highly qualitative analysis was performed with regards to field trends and locations.

This was accomplished by using equivalent material specifications from the aluminum cam and performing varying loads. Graphical effective stress results were then obtained for each loading, using a modified grayscale contour gradient to better approximate the Photoelastic fringe fields. Results were taken and analyzed until sufficient data was present to support the FE equivalency to the Photoelastic results.

Failure Analysis

Failure analysis was performed by examining the effective stress fields for loading values from 10 to 50 kN (2,200 to 11,200 lbs), in addition to two additional tests surrounding the established maximum failure loading of 12.5 kN (~2600 lbs).

Solid Model Generation

The solid model was first imported into the ANSYS interface. Ten-noded, quadratic tetrahedral elements were used for cam components, and eight-noded quadrilateral cubic elements were used for wall generation. The Mesh Tool was utilized to generate a minimal error meshes for all volumes. This was the general procedure for solid element meshes.

Strain Gauge Verification – Solid Model

Results for the solid model strain prediction were performed in an equivalent manner as the planar model, with applied loadings and constraints.

Load steps were also incorporated into the solid model test, writing individual load step files for loads ranging from 100 N to 2kN (25 to 450 lbs) in 200 N increments. The model was then solved using the load steps and the elemental results were obtained using the *List Variables* option of the *TimeHist Postproc*.

Analytical Results

The following is a numerical display of the convergence results for the planar model with respect to element density:

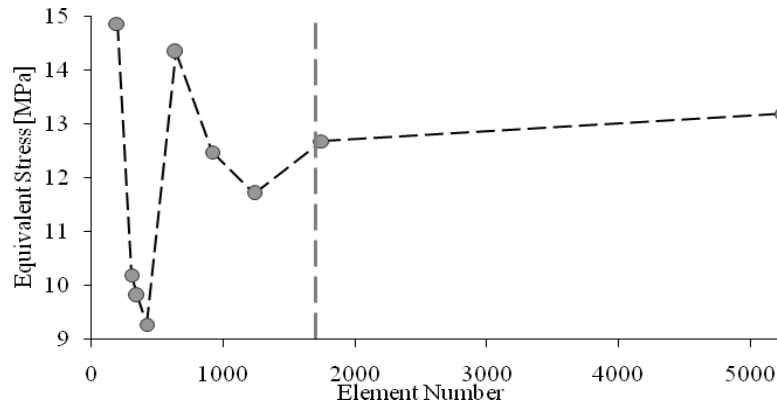
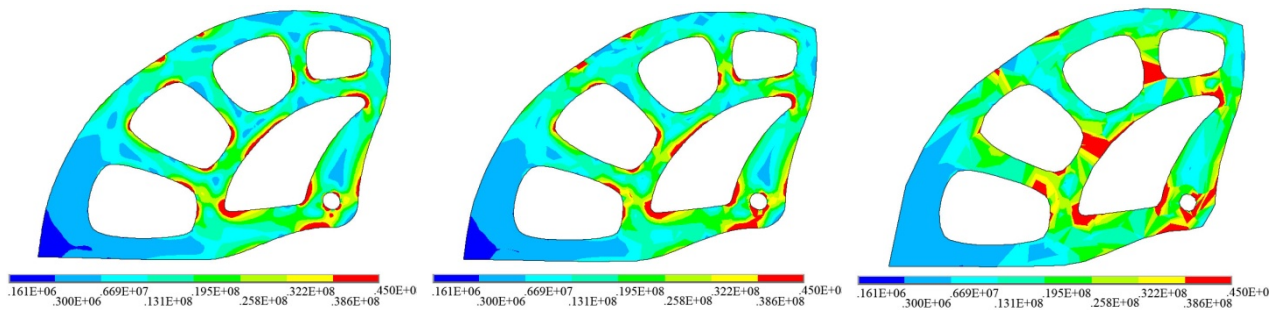


Figure 16: Convergence results for the planar model.

Convergence results were also found to be useful as graphical displays of equivalent stress. The following briefly summarizes these results displaying mesh densities of *Smart Mesh '9'* (198 elements), *Smart Mesh '4'* (640 elements) and the refined mesh of *Smart Mesh '1'* (5247 elements):



Figure

17: Equivalent stress results for three different mesh densities (9, 4 and 1-Refined in order)

The following is also a brief comparison of the mesh choices for Smart Meshes 9 and 1-Refined:

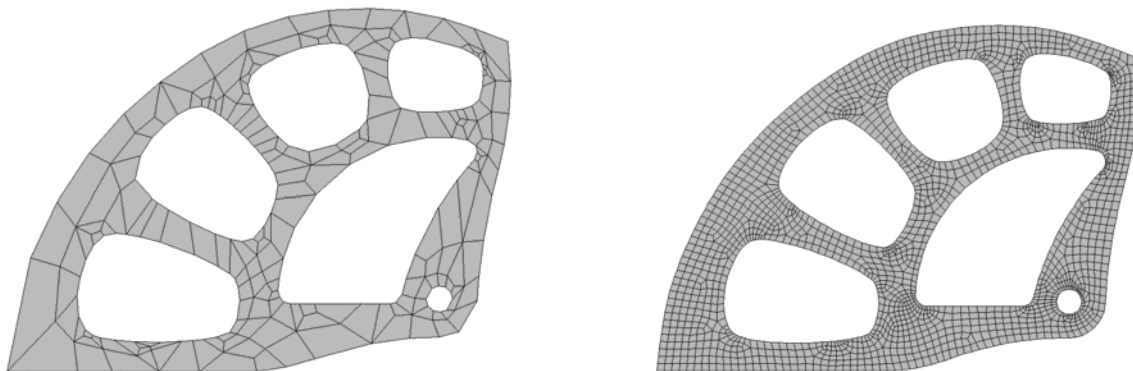


Figure 18: Mesh Densities for Smart Mesh 9 and Smart Mesh 1-Refined.

Next are the equivalent stress results at the gauge location. Presented are the two and three-dimensional approximations as compared to the experimental results:

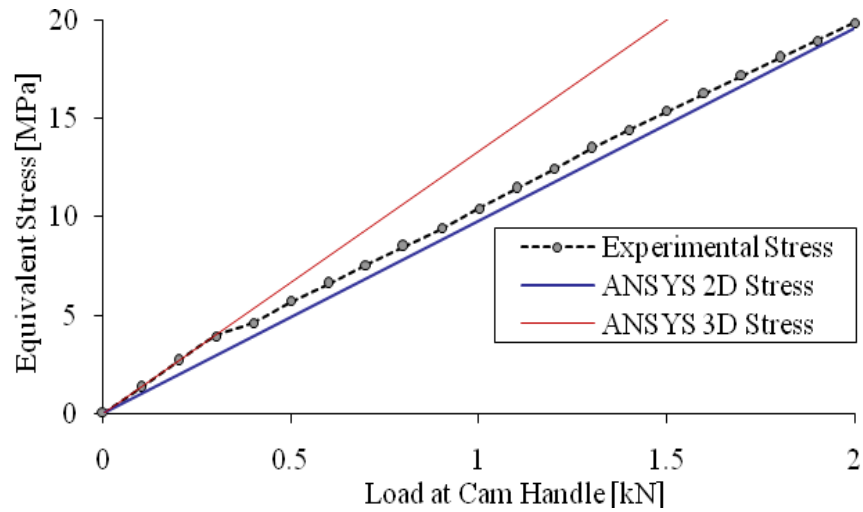


Figure 19: FEA results for equivalent stress at gauge location as compared to experimental results.

The following is a graphical approximation of the internal stress fields as compared to the photoelastic sample. Areas of high similarity are indicated in red:

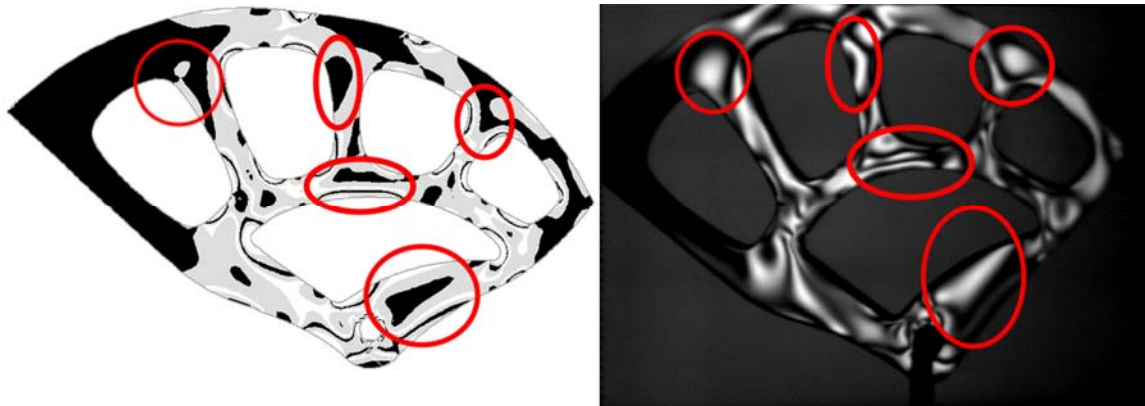


Figure 20: Comparison of the ANSYS stress fields and the photoelastic test stress fields. The red circles indicate similar stress fields. Left: ANSYS stress fields that have been modified in grayscale. Right: Photoelastic test solution.

Numerical scales were omitted from these results due to the highly qualitative nature of this analysis. To note, this grayscale contour utilizes a primary black stress contours in attempt to better model the experimental result of only two fringe fields.

The next figure is a graphical presentation of the equivalent stress at the predicted maximum loading:

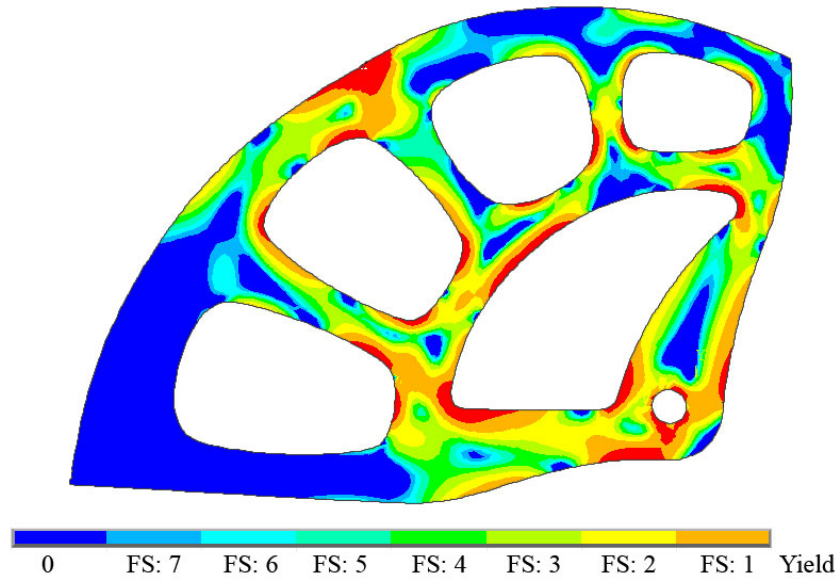


Figure 21: Failure criteria results for maximum loading. Contours represent factors of safety below the yield strength.

See Appendix D for a complete display of the failure results.

Interpretation of Analytical Results

In general, the FE models explored in this analysis provided consistently accurate results. From this result, the primary hypotheses of cam-assembly symmetry and of planar stress in individual cam lobes were verified. However many subtleties of the FE modeling process were also observed, all of which exhibit potential to introduce significant error into the FE results.

The major observation in this analysis was the unnecessary introduction of additional complexity in the three-dimensional model. This addition introduced significantly higher degrees of modeling complexity and load/constraint decisions. This unnecessary addition also created a significantly more expensive solution, which took approximately ten minutes to solve in comparison to the planar models ten second solution time. This factor of sixty in computational time is a strong indicator that increased model complexity should be used only when necessary.

Convergence analysis also presented strong indications that low mesh densities, while predicting roughly the general state of stress across the model, do not model specific areas with much accuracy. This was found to be a factor of the stress discontinuities presented at the element surfaces, and also the low degree of symmetry found in most low-density type elements. Thus it was expected that as the element density was increased, fields generally became smoother in appearance.

Photoelastic analysis also proved to be difficult in absence of material specifications that would indicate the specific stress field values found in the experiment. Ultimately it was found that numeric approximations of these fields were unobtainable with any degree of accuracy without this data. However through extensive empirical examination, it was found that qualitative analysis with regards to stress field propagations and concentrations was possible.

Discussion

The solutions obtained from ANSYS were compared to the data gathered from the experimental test. The effective stress at the strain gage location for various cam handle loads is shown in Fig. 21. The results show a very close solution for the 2D ANSYS solution. The 3D ANSYS solution is not as close to the values obtained experimentally.

The error in the 3D ANSYS model prediction for the effective stress is most likely attributed to selecting the wrong location for the values of effective stress. The stress field along the web of the cam is not constant and the stresses are highly sensitive to the location. Selecting a slightly different location for the stress can result in drastically different stress values. This source of error could be present for the 2D solution.

Experimental test conducted to verify the ANSYS solution focused on obtaining exact numbers for single point on the cam. It provided accurate numbers for a specific region. Verifying the solution for a specific point does help validate the ANSYS solution but it does not automatically mean that the ANSYS solution is correct for other areas. For this reason, a more qualitative photoelastic test was conducted to verify the ANSYS solution for all regions. The photoelastic test did not provide accurate values of strains or displacement, but it did provide a visualization of the stress field. Both verification methods were important in validating the ANSYS solution.

Fig. 21 shows the internal stress fields predicted by ANSYS and the stress fields obtained through the photoelastic test. Numerical scales were omitted from these results due to the highly qualitative nature of this analysis. To note, this grayscale contour utilizes to primary black stress contours in attempt to better model the experimental result of only two fringe fields.

There are many similar stress region produced between the photoelastic test and the ANSYS solution as shown in red circles in Fig. 21. The areas that are dissimilar are areas that have very complex stress fields. Complex stress fields are harder to interpret and compare. For this reason, the areas that have dissimilar stress fields do not necessarily invalidate the ANSYS results. Overall, the photoelastic test validates the ANSYS solution.

The major observation in this analysis was the unnecessary introduction of additional complexity in the three-dimensional model. This addition introduced significantly higher degrees of modeling complexity and load/constraint decisions. This unnecessary addition also created a significantly more expensive solution, which took approximately ten minutes to solve in comparison to the planar models ten second solution time. This factor of sixty in computational time is a strong indicator that increased model complexity should be used only when necessary.

Convergence analysis also presented strong indications that low mesh densities, while predicting roughly the general state of stress across the model, do not model specific areas with much accuracy. This was found to be a factor of the stress discontinuities presented at the element surfaces, and also the low degree of symmetry found in most low-density type elements. Thus it was expected that as the element density was increased, fields generally became smoother in appearance.

There are many sources of error. The computer model was created from measurements of various points on the physical cam. The measurements were not perfectly accurate. The geometry difference between the physical and computer model of the cam is a source of error. Also, during the experimental test, the measured force was not constant. The Instron was manually adjusted to maintain a constant force on the climbing cam while the strain data was collected.

In the ANSYS material modeling, a linear elastic, homogenous, isotropic material behavior was assumed. The material model assumptions simplify the solution but it introduces sources of error. A constant modulus of elasticity and a constant poisson ratio was used. Realistically, no material has a perfectly homogenous material property. Also, the climbing cam as tested most likely does not have the exact material property as given by Matweb. This would result in a different stress solution than observed in the experimental test. Assuming a linear elastic behavior is appropriate since during experimental test, the cam did not reach the plastic region. Though the material modeling simplification introduce sources of error, it is appropriate since it does not drastically affect the final solution.

Failure Analysis

Using the established maximum loading scenario for a two-hundred pound climber falling from a height of thirty feet with seven percent rope-stretch, a maximum impact loading of 2,850 pounds was established. This is the equivalent of approximately fourteen vertical G's of acceleration, and represents a worst case scenario for climbing accidents before fatality and/or severe injury become more significant factors.

Examination of stress fields in individual cam lobes using safety factors as a quality of measure, it was found that this load presented only minor plastic deformation in the cam apparatus. Given sufficient friction to hold the apparatus in place, it should then adequately withstand this impact, but would most likely require replacement afterward.

It was also found that this impact region surrounding 3,000 pounds also signified the region for which the cam began entering a significant state of plastic deformation across the specimen. Loads exceeding approximately 3,400 pounds were found to present general states of complete failure in individual cam lobes. It is hypothesized from this result then that the cam lobe was optimized for weight by the cam engineers. This is also supported by the climbing communities' strong emphasis on using light-weight climbing gear.

In conclusion of the FE analysis, it was found that loads exceeding approximately 2,500 pounds presented a factor of safety of two throughout the cam device and is safe for continued use. This is matched also using the manufacturer's recommended maximum loading of 3,200 pounds.

Conclusion

The FE models explored in this analysis provided solutions consistent with the validation tests. The 2D model solution closely matched the value obtained in the experimental test. The stress fields developed in the photoelastic test closely resembled the stress fields predicted by ANSYS. Future experiments should test the climbing cams to failure to determine the location and method of failure. Also, measuring the strains at multiple points on the cam during experimental testing would provide more insight into the accuracy of the FE solution.

Appendices Listing

APPENDIX A: REFERENCES

APPENDIX B: STRAIN GAGE DATA FROM EXPERIMENTAL TEST

APPENDIX C: DISCUSSION OF MAXIMUM LOADING SCENARIO

APPENDIX D: DISCUSSION OF MODEL LOADING AND CONSTRAINTS

APPENDIX E: SUMMARY OF FAILURE RESULTS

APPENDIX F: WORK DIVISION

APPENDIX A: REFERENCES

“Aluminum 7075.” Matweb. 2007. 15 Nov. 2007 <<http://www.matweb.com/search/DataSheet.aspx?MatID=9596>>

Custer, Dave. “An Elastic Model of the Holding Power of Spring Loaded Camming Devices Used as Rock Climbing Anchors.” MIT. December 5, 2007. <http://web.mit.edu/custer/www/rocking/cams/cams.body.html#fig3>

Doyle, James F., and James W. Phillips. Manual on Experimental Stress Analysis. 5th ed. Society for Experimental Mechanics, 1989.

Logan, Daryl L. A First Course in the Finite Element Method. United States: Thompson, 2007.

APPENDIX B: STRAIN GAGE DATA FROM EXPERIMENTAL TEST

Table B: Strain gage data. Values averaged for each load step.

Force	e(1)	e(2)	e(3)
0	0	-0.7	-0.9
100	12.6	-12	-36.2
200	25.9	-24	-74.1
300	38.6	-35.2	-109.2
400	46.5	-41.2	-129.1
500	56.2	-50.4	-158.6
600	65.7	-58.3	-184.2
700	75	-67	-210.7
800	83.7	-75.6	-236
900	93.1	-84	-262.2
1000	102.2	-92.3	-289.4
1100	111.5	-100.9	-316.6
1200	120.2	-108.5	-343.3
1300	129.3	-116.4	-370.7
1400	137.9	-124.4	-396.2
1500	146	-131.6	-421.6
1600	154.2	-139.4	-446
1700	161.9	-145.8	-469.8
1800	169.9	-152.3	-493.5
1900	177.4	-159.1	-516.4
2000	184.8	-165.7	-539.8
2100	192.2	-171.8	-561.7

APPENDIX C – DISCUSSION OF MAXIMUM LOADING SCENARIO

The following is a schematic illustrating a climbing fall Scenario:

Load capabilities for climbing gear are set by The International Mountaineering and Climbing Federation (UIAA). Limited data was available regarding specific standards due to website maintenance; however the following criteria were still obtained from other sources.:

- The UIAA establishes loading criteria for dynamic climbing rope. These maximum loading criteria for climbing rope then dictate the maximum loading criteria for climbing gear.
- The UIAA has several standards for rope. There are two specific standards that effect climbing gear design:
 - Withstand five falls of a 1.71 fall factor for an 80 kg person.
 - Provide no more than 12 kN of impact for an 80 kg person with a fall factor of 2.

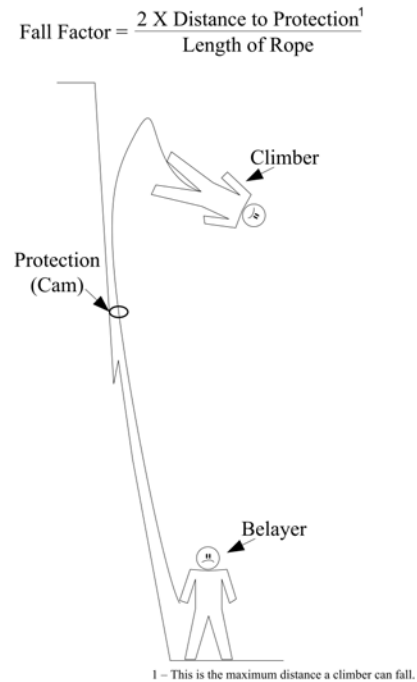


Figure 22: Climbing Fall Scenario

From these criteria we than can establish failure criteria for the cam device. They are as follows for the cam device:

- Withstand 12 kN load at handles (13 kN load on individual lobes)
- Withstand five repeated loads of 10.25 kN (11 kN on individual lobes)

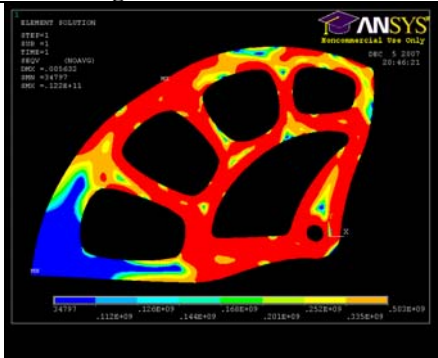
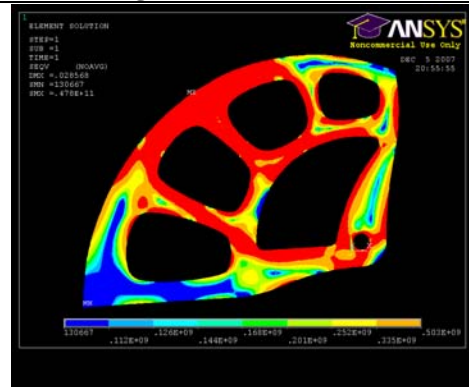
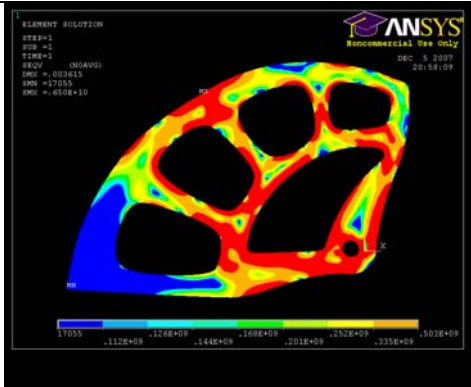
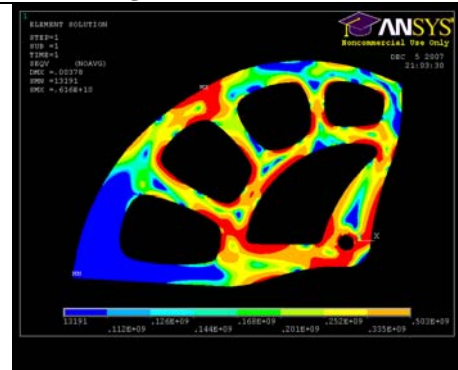
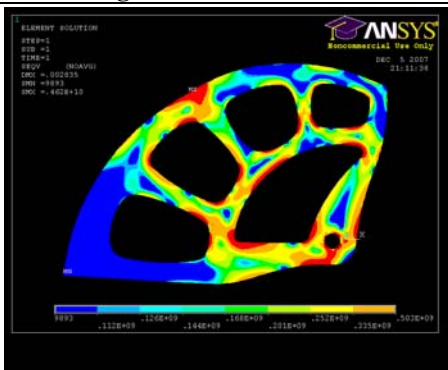
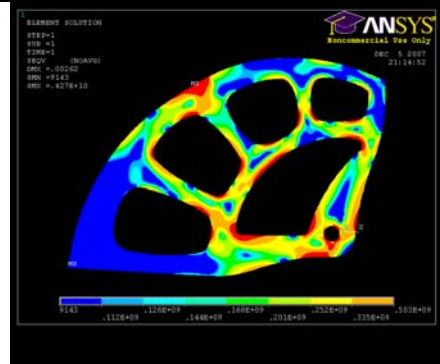
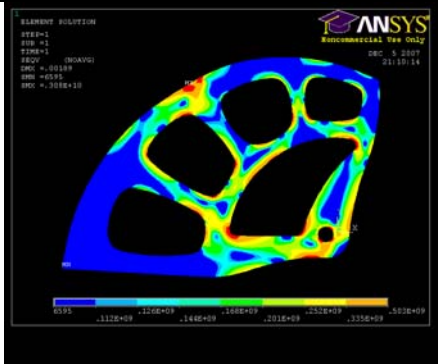
With these we can then analyze the cam lobe for failure based on yielding and fatigue criteria. A fatigue criterion was omitted from FE analysis as it is outside the scope of this class.

Additional Notes:

- Shock loading from a fall is of three factors:
 - Energy absorption of rope
 - Fall factor (Length of Rope/Length of Fall)
 - Weight
- Dynamic Climbing Rope exhibits typical rope stretch of 6-10%

APPENDIX D – SUMMARY OF FAILURE RESULTS

The following are graphical results of the effective stress fields for various loadings:



APPENDIX D – SUMMARY OF FAILURE RESULTS

The following are the work divisions on this project.

Project Section	
Strain Gauge Test/Apparatus	David, Matt
Photoelastic Test	All
Cam Solid Modeling	David
FEA Testing	Justin

Report Section	Member(s)
Intro	David
Exp Proc	Matt, David
Exp Results	Matt, David
Analy Metho	Justin
Analy Proc	Justin
Analy Results	Justin
Interpretation of Analy Results	Justin
Failure Analy	Justin
Discussion	Matt
Conclusion	Matt
Appendix C	Justin